Ⓔ

A PLANET AT 5 AU AROUND 55 CANCRI[1]

GEOFFREY W. MARCY,[2,3] R. PAUL BUTLER,[4] DEBRA A. FISCHER,[2] GREG LAUGHLIN,[5] STEVEN S. VOGT,[5]
GREGORY W. HENRY,[6] AND DIMITRI POURBAIX[7]

ABSTRACT

We report precise Doppler-shift measurements of 55 Cancri (G8 V) obtained from 1989 to 2002 at Lick Observatory. The velocities reveal evidence for an outer planetary companion to 55 Cancri orbiting at 5.5 AU. The velocities also confirm a second, inner planet at 0.11 AU. The outer planet is the first extrasolar planet found that orbits near or beyond the orbit of Jupiter. It was drawn from a sample of ~50 stars observed with sufficient duration and quality to detect a giant planet at 5 AU, implying that such planets are not rare. The properties of this Jupiter analog may be compared directly to those of the Jovian planets in our solar system. Its eccentricity is modest, $e = 0.16$, compared with $e = 0.05$ for both Jupiter and Saturn. Its mass is at least 4.0 $M_{\rm JUP}$ ($M \sin i$). The two planets do not perturb each other significantly. Moreover, a third planet of sub-Jupiter mass could easily survive between these two known planets. Indeed, a third periodicity remains in the velocity measurements with $P = 44.3$ days and a semiamplitude of 13 m s^{-1}. This periodicity is caused either by a third planet at $a = 0.24$ AU or by inhomogeneities on the stellar surface that rotate with period 42 days. The planet interpretation is more likely, as the stellar surface is quiet both chromospherically [$\log(R'_{\rm HK}) = -5.0$] and photospherically (brightness variations less than 1 mmag). Moreover, any hypothetical surface inhomogeneity would have to persist in longitude for 14 yr. Even with all three planets, an additional planet of terrestrial mass could orbit stably at ~1 AU. The star 55 Cancri is apparently a normal, middle-aged main-sequence star with a mass of 0.95 $M_\odot$, rich in heavy elements ([Fe/H] = +0.27). This high metallicity raises the issue of the precise relationship between its age, rotation, and chromosphere.

Subject headings: planetary systems —
  stars: individual (55 Cancri, HIP 43587, HD 75732, HR 3522, ρ^1 Cancri)

On-line material: machine-readable table

1. INTRODUCTION

Rarely in modern astrophysics does a nearby star attract intense scrutiny on three observational fronts. The main-sequence star 55 Cancri (=ρ^1 Cnc = HD 75732 = HIP 43587 = HR 3522, G8 V) has been examined for its high abundances of chemical elements, its close-in orbiting planet, and its controversial disk of dust. These three putative properties are plausibly linked together by the formation and evolution of planetary systems, making the system rich with implications.

The metal-rich nature of 55 Cnc was first noticed by H. Spinrad & B. Taylor, who alerted Greenstein & Oinas (1968). They all noted its unusually high abundance of iron and carbon relative to that in the Sun. The iron lines and CN molecular absorption spectral feature were particularly prominent in blue photographic spectra. These results were confirmed by Taylor (1970) and, indeed, Bell & Branch (1976) reported that carbon was yet further enhanced over iron, [C/Fe] = +0.15. Later spectral analyses of 55 Cnc have confirmed its high metallicity (Cayrel de Strobel et al. 1992, 2001; Taylor 1996; Gonzalez & Vanture 1998; Feltzing & Gonzalez 2001) with estimates of (logarithmic) iron abundance relative to the Sun in the range [Fe/H] = +0.1–0.5. Thus 55 Cnc is regarded as a rare "super–metal-rich" main-sequence star, but confusion still remains about the interpretation of these stars (Taylor 2002, Reid 2002).

A planet was reported around 55 Cnc having an orbital period of 14.65 days, an implied orbital radius of 0.11 AU, and a minimum mass of $M \sin i = 0.84$ $M_{\rm JUP}$ (Butler et al. 1997). It was the fourth extrasolar planet discovered, coming after the planets around 51 Peg, 70 Vir, and 47 UMa. The velocity residuals to the orbital fit of 55 Cnc exhibited a monotonic increase of 90 m s^{-1} from 1989 to 1995 followed by an apparent decrease in 1996. Butler et al. noted that these residuals constrained a possible second planet to have a period $P > 8$ yr and a mass $M \sin i > 5$ $M_{\rm JUP}$. The decrease in the velocity residuals continued during 1997 (Marcy & Butler 1998), supporting the planetary interpretation. However, with neither a full orbital period nor a Keplerian velocity curve, the possibility of stellar activity as the cause of the residuals could not be excluded. This star joined 51 Peg (Mayor & Queloz 1995; Marcy et al. 1997) as members of a growing class of planet-bearing stars that have metallicity well above solar (Gonzalez 1998; Barnes 2001; Santos 2000; Butler et al. 2000).

A third issue arose for 55 Cnc when Dominik et al. (1998) presented evidence for a Vega-like dust disk based on *Infrared Space Observatory* (*ISO*) measurements between 25 and 180 μm. They detected the photosphere at 25 μm and excesses at the higher wavelengths. Trilling & Brown (1998) reported resolving the disk out to 3″2 (40 AU) with near-infrared coronographic images. Controversy over the disk detections arose when Jayawardhana et al. (2000) found the submillimeter emission to be lower by a factor of 100 than that expected from the disk reported by Trilling & Brown. Equally troubling were observations by the NICMOS near-infrared camera on the *Hubble Space Telescope* (*HST*) (Schneider et al. 2001) that imposed an upper limit on the near-infrared flux that was 10 times lower than that reported by Trilling & Brown. A possible resolution of the discrepancies was provided by Jayawardhana et al. (2002), who found three faint sources of submillimeter emission that were located near but not centered on 55 Cnc, implying that past detections of IR flux might have come from background objects. The NICMOS upper limit, the upper limit to the submillimeter flux, and the detection of background field sources suggest that no disk has been detected around 55 Cnc. Indeed, Habing et al. (2001) discuss the nonnegligible probability of spurious detections of disks by *ISO* caused by fluctuations and by background field sources.

The star 55 Cnc is also a visual binary, with a common proper motion companion 7 mag fainter ($V = 13$, $I = 10.2$), separated by 85″ corresponding to 1100 AU projected on the sky (Hoffleit 1982). We have measured the barycentric radial velocities for components A and B to be 27.3 ± 0.3 and 27.4 ± 0.3 km s^{-1}, respectively (Nidever et al. 2002). Thus, the two common proper motion stars are indeed likely bound. Their common space motion is similar to that of the Hyades supercluster (Eggen 1993).

This paper will be concerned only with component A, which we will refer to as " 55 Cnc " and for which we report continued radial velocities measurements extending from 1989 to 2002.4. In § 2 we provide an update on the properties of the star, especially its mass, metallicity, and chromospheric activity level. In § 3 we present all the radial velocity measurements, and § 4 contains the orbital fit to two planets. In the remaining sections we study the possibility of additional planets and the gravitational dynamics between the planets.

2. PROPERTIES OF 55 CNC

2.1. *Stellar Surface Temperature, Metallicity, and Mass*

The inferred value of the minimum mass for the planet, $M \sin i$, scales with the two-thirds power of the adopted mass of the host star (plus companion). Unfortunately, the mass and evolutionary status of 55 Cnc remain uncertain despite many spectroscopic analyses. The mass is best derived from stellar evolution models constrained by the observed luminosity, metallicity, and effective temperature of the star.

The absolute visual magnitude of 55 Cnc is 5.47 ± 0.05, yielding a luminosity of $0.61 \pm 0.04\ L_\odot$ from the *Hipparcos* parallax of 79.8 ± 0.84 mas (Perryman et al. 1997). Coupled with its color, $B-V = 0.87$, and spectral type of G8 V, the star resides a few tenths of a magnitude brighter than the zero-age main sequence. The star's color, spectral type, and luminosity render it as a normal main-sequence star of

modest age, a few gigayears. If it had solar metallicity, its inferred mass would be 0.92 $M_\odot$ (Allende Prieto & Lambert 1999).

The metallicity of 55 Cnc, however, is certainly above solar. Various LTE analyses of high-resolution spectra of 55 Cnc have yielded measured metallicities in the range [Fe/H] = 0.20–0.45 (Fuhrmann, Pfeiffer, & Bernkopf 1998; Gonzalez & Vanture 1998; Baliunas et al. 1997; Taylor 1996; Arribas & Martinez-Roger 1989; Perrin et al. 1977; Oinas 1977; Feltzing & Gonzalez 2001). These same LTE analyses yield measurements of the effective surface temperature that fall in the range $T_{\rm eff} = 5100$–5340 K, in agreement with the spectral type of G8 V. Two excellent reviews of the atmospheric analyses and interior models for 55 Cnc are provided by Ford, Rasio, & Sills (1999) and by Henry et al. (2000).

The above uncertainties in $T_{\rm eff}$ and [Fe/H] leave the inferred stellar mass, derived from evolutionary models, uncertain by $\sim$10%. An additional evolutionary constraint can be imposed by age estimates, derived from the Ca II H and K chromospheric emission, the star's position on theoretical evolutionary tracks in the H-R diagram, and its Galactic space motion. The mean H and K emission level during 6 yr implies an age of 4.5 ± 1 Gyr (Donahue 1998; Henry et al. 2000). The age estimates from the star's placement on evolutionary tracks range from 1 Gyr (Fuhrmann et al. 1998) to 8 Gyr (Ford et al. 1999; Gonzalez 1998). This lack of precision in age dating is disturbing and is caused primarily by the poor atmospheric parameters of $T_{\rm eff}$ and [Fe/H]. The star is variously suggested to be a subgiant or a zero-age main-sequence member of the Hyades moving group (Fuhrmann et al. 1988; Eggen 1993; Deltorn & Kalas 2002). The space motion velocity of 55 Cnc relative to the LSR is 29.5 km s^{-1} (Reid 2002), similar to disk stars of modest age, 2–8 Gyr. The modest precision of the $T_{\rm eff}$ and age of 55 Cnc suggests that our astrophysical understanding of simple main-sequence stars leaves room for advancement.

We have independently carried out a preliminary LTE analysis for 55 Cnc based on Keck/HIRES and Lick/Hamilton spectra at resolution 60,000. Details will appear in D. A. Fischer & J. Valenti (2003, in preparation). We find $T_{\rm eff} = 5240 \pm 50$ K, which falls in the middle of the range of previous measurements. Our LTE analysis yields [Fe/H] = $+0.27 \pm 0.03$ for 55 Cnc. We also find that other elemental abundances are enhanced over solar with C, Si, S, Ca, and Ni $\sim$0.3 dex above solar (D. A. Fischer & J. Valenti 2003, in preparation). Thus 55 Cnc is not only metal-rich in iron-peak elements but even more enriched in alpha elements.

Our metallicity of [Fe/H] = $+0.27$ resides in the lower half of the metallicity estimates from other groups. A new calibration of metallicity based on *uvby* photometry has been carried out by Martell & Laughlin (2002) and rests on 1533 calibration stars drawn from the Hauck-Mermilliod (1998) *uvby* catalog and the Cayrel de Strobel (1992) spectroscopic metallicity catalog. This calibration applied to 55 Cnc gives [Fe/H] = $+0.29 \pm 0.12$ and $T_{\rm eff} = 5220 \pm 80$ (Martell & Laughlin 2002), in agreement with our LTE spectroscopic analysis. The *uvby*-based metallicity estimate of Schuster & Nissen (1989) is [Fe/H] = $0.10 + / - 0.16$.

We conclude that 55 Cnc is metal-rich with [Fe/H] = $+0.27 \pm 0.10$. Compared to stars in the solar neighborhood, 55 Cnc is metal-rich, residing $\sim$2 standard deviations from the mean metallicity (Santos, Israelian, & Mayor 2001; Reid 2002; Butler et al. 2000). That is, 5% of the stars in the

solar neighborhood have larger [Fe/H]. This more modest metallicity ameliorates the difficulties in modeling the evolutionary status of 55 Cnc (see Ford et al. 1999 and Fuhrmann et al. 1998 for past inconsistencies). The problem was that models predict a main sequence for stars having [Fe/H] $\sim +0.4$ that is simply more luminous than 55 Cnc actually is, near $T_{\mathrm{eff}} \approx 5250$ K. There is no plausible evolutionary explanation for a star to reside below the main sequence, unless in fact its metallicity is lower. Indeed, evolutionary models with [Fe/H] $= 0.27$ exhibit a lower (less luminous) main sequence in the H-R diagram, allowing a self-consistent solution for 55 Cnc with a mass of 0.9–1.0 $M_\odot$ and an age of 2–8 Gyr, similar to the age derived from the H and K chromospheric emission level and its Galactic kinematics.

Two recent mass estimates of 55 Cnc from evolutionary models yield 0.95 $M_\odot$ (Ford et al. 1999) and 1.08 $M_\odot$ (Fuhrmann et al. 1998). Here we estimate the mass of 55 Cnc from its observed luminosity, T_{eff}, H and K–derived age of 5 Gyr (Henry et al. 2000), and the new [Fe/H] value of $+0.27$. We use the set of interior models provided by Ford et al. (1999), extrapolated from [Fe/H] of $+0.39$ to $+0.27$. We find a good fit to all observed parameters occurs for a mass of 0.95 $M_\odot$, the same as found by Ford et al. (1999). We therefore adopt a mass for 55 Cancri of 0.95 ± 0.1 $M_\odot$.

2.2. *Stellar Rotation*

The Ca II H and K chromospheric emission provides two separate determinations of the axial stellar rotation. A predicted rotation period can be determined from the color index ($B-V$) and average Ca II flux index, $\langle S \rangle$ (Noyes et al. 1984). Henry et al. (2000) report $\langle S \rangle = 0.19$ during 6 yr of monitoring, implying a predicted rotation period of 42.2 days. We have obtained five spectra of the Ca II K line of 55 Cnc from the Keck observatory using the HIRES spectrometer (Vogt et al. 1994). A representative spectrum near the K line at 393 nm is shown in Figure 1. The weak emission reversal in the line core is visible to the eye, indicating that the star has a weak to modest chromosphere and is thus relatively old (Noyes et al. 1984). All five Keck spectra yield $S = 0.18$ within 0.02, in agreement with the value given by Henry et al. Independently, actual periodicities have been detected in the H and K emission caused by magnetically active regions on the stellar surface that rotate into and out of the visible hemisphere (Baliunas et al. 1985). Periods of 35–43 days have been detected for 55 Cnc (Henry et al. 2000).

This observed rotation period might vary with the phase of the magnetic stellar cycle, as the fields migrate in latitude à la the butterfly diagram for the Sun (Donahue, Saar, & Baliunas 1996). Based on the Sun, we expect rotation periods to vary by up to 10% on other G dwarfs as the magnetic regions migrate in latitude. The rotation period of 35–43 days represents some unknown range of latitudes on the surface of 55 Cnc during the era from 1993–2000 when the H and K observations were made (Henry et al. 2000).

This range for the rotation period of 55 Cnc, 35–43 days, is unlikely to be grossly in error since it stems from actual periodicities in emission and the range agrees with the rotation period from the mean H and K level (42 days). Nonetheless, the high metallicity of 55 Cnc raises some concern about the integrity of the Noyes calibration of rotation period with mean S value. Soderblom (1985) has used the Hyades stars to test the effects of high metallicity on the standard correlations between S value, $B-V$, and stellar rotation given by Noyes et al. (1984). The Hyades has [Fe/H] $= +0.15 \pm 0.05$, and many stars have rotation rates directly measured from photometric periodicities (Lockwood et al. 1984). Apparently, Hyades dwarfs have longer rotation periods (slower spin rates), by about 10% compared to stars of solar metallicity (Soderblom 1985). Thus for the metal-rich 55 Cancri, the predicted rotation period of 42.2 days may be an underestimate of its true rotation period by 10%–15%. If so, the predicted rotation period would be 46–50 days, somewhat above the range of actual observed periodicities. Clearly, a detailed study of the calibration of activity versus stellar rotation for different metallicities is needed.

Stellar rotation can also be detected photometrically. Differential Strömgren photometry with the T8 0.8 m automatic photoelectric telescope (APT) at Fairborn Observatory (Henry 1999) has been carried out over the past 6 yr. Figure 2 shows the results in the combined Strömgren
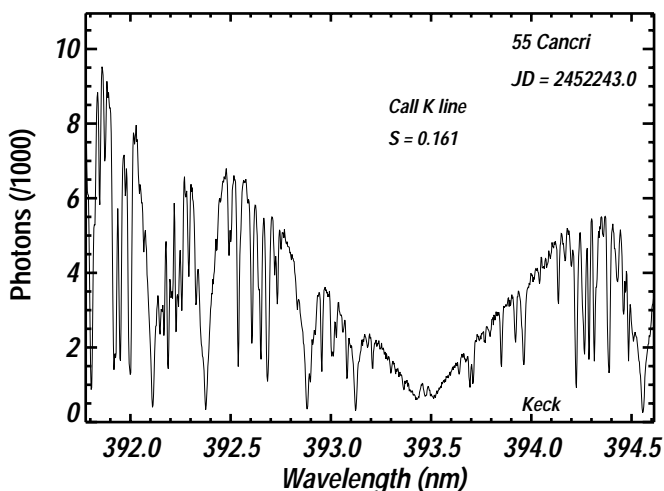

FIG. 1.—Spectrum of 55 Cancri near the Ca II K line showing the modest central emission reversal in the core. The star is relatively quiescent, typical for a middle-aged star, with a Mount Wilson chromospheric index of $S = 0.16$. The deep absorption lines visually reveal the high metallicity, found here to be [Fe/H] $= +0.27$. This metallicity along with its luminosity and T_{eff} implies a stellar mass of 0.95 $M_\odot$.
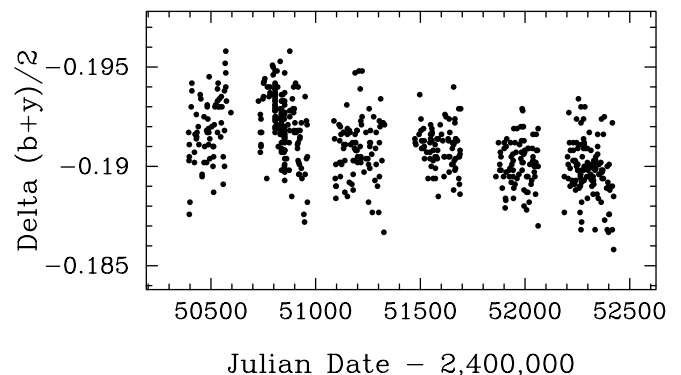

FIG. 2.—Differential Strömgren photometry of 55 Cnc during the past six observing seasons acquired with a 0.8 m APT. The night-to-night rms is ~ 1.2 mmag within each season, consistent with the usual measurement precision. A downward trend of 2 mmag over the 6 yr indicates a modest magnetic cycle, typical for a middle-aged G8-type main-sequence star.

$(b + y)/2$ passband. The photometry reveals a gradual decline in mean brightness of 0.002 mag.

The downward trend is undoubtedly due to long-term changes in the level of magnetic activity, normal for middle-aged, inactive stars. We have also computed a power spectrum of the photometry. For a brief discussion of the method see Henry et al. (2001). Not surprisingly, given the star's low level of activity, we find no hint of any periodicity between 2 and 100 days. We get similar results when we analyze each observing season separately. The individual seasonal light curves all show night-to-night constancy of 0.0012 mag, the limit of photometric precision for a single observation.

When we phase the entire data set with a prospective 44.3 day period (see § 6) and do a least-squares sine fit, we get a semiamplitude of 0.00018 ± 0.00009 mag, which constitutes a nondetection. Similarly, we find no signal at the 0.005 mag level when folding the 108 *Hipparcos* photometric measurement of 55 Cnc at periods near 44.3 days.

These photometric results suggest that the star is middle-aged and chromospherically inactive. By comparison with similar G dwarfs being monitored for Doppler-shift variations, 55 Cnc stands as a quiescent star and is expected to exhibit velocity jitter of 3–5 m s^{-1} (Saar et al. 1998; Santos et al. 2000) due to surface effects. Jitter cannot be accurately predicted, but such quiet stars always exhibit jitter less than 5 m s^{-1}. Moreover, no periodicities appear other than the Ca II H and K variations at the rotation period of 35–43 days.

Rotation can also be assessed from high-resolution spectra to reveal Doppler broadening of the absorption lines. For 55 Cnc, estimates of $V \sin i$ lie between 1.0 and 1.5 km s^{-1} (Soderblom 1982; Fuhrmann et al. 1998) with uncertainties of ~0.5 km s^{-1}. For a likely radius of the star of 0.95 $R_\odot$, the measured rotation period of 35–43 days implies an equatorial velocity of 1.3 ± 0.1 km s^{-1}, consistent with the measured values of $V \sin i$. Since the Ca II H and K rotational periodicity is so clearly seen (Henry et al. 2000), the viewing angle of the star cannot be nearly pole-on. Indeed, viewing angles near pole-on occur rarely from a statistical standpoint. These arguments suggest that the star is viewed within ~45° of the equator. Note, however, that $V \sin i$ is too poorly measured to extract $\sin i$ directly from known rotation period and stellar radius.

In summary, 55 Cnc is a metal-rich, middle-aged main-sequence star with a mass of 0.95 $M_\odot$. Its chromospheric emission and photometric variability are both low, similar to the majority of middle-aged G8 dwarfs, all of which are photospherically stable. The stellar characteristics of 55 Cnc are listed in Table 1. These characteristics all fall within the normal range found for middle-aged G8 main-sequence stars. We expect its surface behavior, especially photospheric velocity "jitter," due to surface turbulence and spots, to be 3–5 m s^{-1} for such a star (Saar et al. 1998; Saar & Fischer 2000; Santos et al. 2000). Indeed, among 1,200 FGKM dwarfs that we are studying with precise velocities, we find the velocity jitter to be 3 ± 2 m s^{-1} for such middle-aged, photometrically quiet stars.

3. RADIAL VELOCITY OBSERVATIONS

We have obtained 143 measurements of the velocity of 55 Cnc, during 13 yr from 1989 to 2002. Spectra were obtained with the cross-dispersed echelle spectrometer, the

TABLE 1
STELLAR PROPERTIES OF
55 CANCRI

Parameter	Value
Spectral type	G8 V
V (mag)......................	5.95
$B-V$ (mag)................	0.87
$M_{Star} (M_\odot)$	0.95
$\log(R'_{HK})$	−5.02
[Fe/H]	+0.27
Distance (pc).............	12.53
P_{Rot} (day)..................	35–42
Age (Gyr)..................	3–8

"Hamilton" (Vogt 1987). We placed a special-purpose iodine absorption cell in the stellar path to provide calibration of both wavelength and the spectrometer point-spread function (PSF) (Butler et al 1996). The iodine absorption cell has remained the same during the entire 13 yr and is always temperature controlled to 50 ± 0.1 C. As the Pyrex cell is glass sealed, the column density of iodine remains the same, and the iodine line widths have remained constant during the 13 yr. The dense forest of iodine absorption lines provides an indelible record of the wavelength scale and behavior of the spectrometer at the instant of each observation (Butler et al. 1996).

The starlight was gathered with the 3 m "Shane" and 0.6 m "CAT" telescopes, both of which feed the Hamilton spectrometer. The resolution of the Hamilton was $(\lambda/\Delta\lambda) = 40,000$ from 1989 to November 1994. Starting 1994 November, the Hamilton camera optics were improved by installing a new corrector plate and new field flattener. The new PSF has reduced wings and is more symmetric. At that same time, the wavelength coverage was expanded with a larger CCD, from 800^2 to 2048^2 pixels. These improvements yielded a resolution of 55,000 and higher Doppler precision by a factor of ~2.5.

The Doppler shifts of all spectra were determined by synthesizing the composite spectrum composed of the star and iodine lines. The free parameters in each 2 Å chunk of spectrum included the linear wavelength scale, the spectrometer PSF, and the Doppler shift. A complete description of our Doppler analysis is given by Butler et al. (1996).

Velocity measurements for three arbitrary comparison stars of spectral type G and K, similar to 55 Cnc, are shown in Figure 3. These stars were observed with the same Hamilton spectrometer and telescopes at Lick Observatory as was 55 Cnc. The stability of the Doppler measurements over the decade is apparent, with scatter ~10 m s^{-1} or less and no trends over the long term. This suggests that the measurements carry no systematic errors greater than 10 m s^{-1}.

The velocity measurements are listed in Table 2 and shown in Figure 4. The first 14 Doppler measurements made between 1989 and 1994 November have uncertainties of typically 8–10 m s^{-1}, worse than most of the subsequent observations, due to the unrepaired optics of the Hamilton spectrometer. They have not been inflated by ~30% as suggested by Cumming, Marcy, & Butler (1999). Observations made since 1994 December have uncertainties of typically 3–5 m s^{-1}.

The standard deviation of the velocities is 69 m s^{-1}, with peak-to-peak variations of 280 m s^{-1}. These velocity
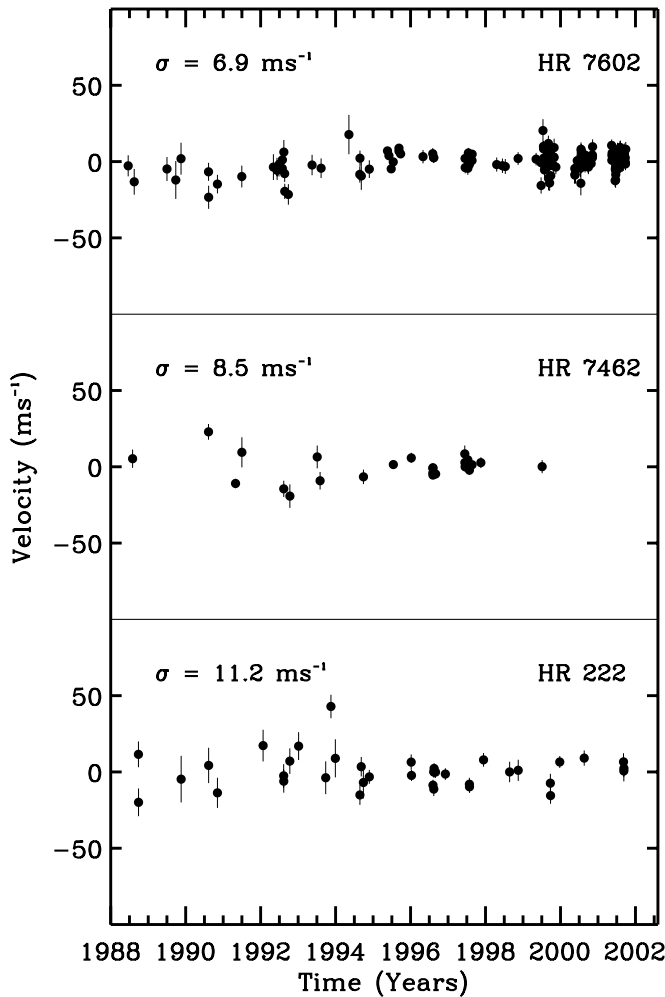
FIG. 3.—Comparison stars. Doppler-shift measurements for three different GK dwarfs observed from 1989 to present taken with the same instrumental setup and the Lick telescopes. These stars demonstrate Doppler precision and long-term stability at a level of 10 m s^{-1}.
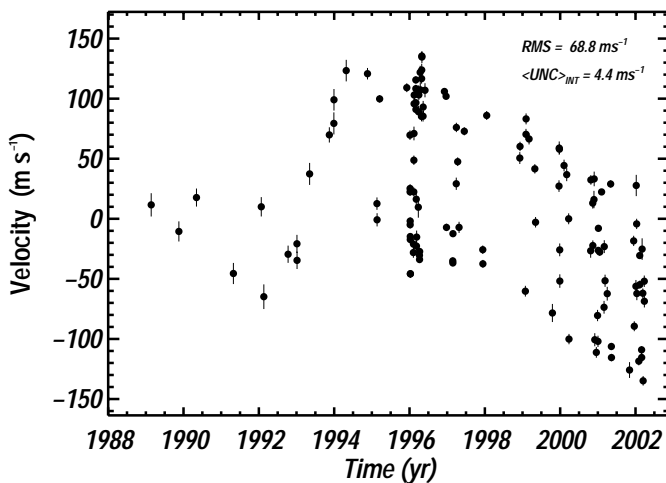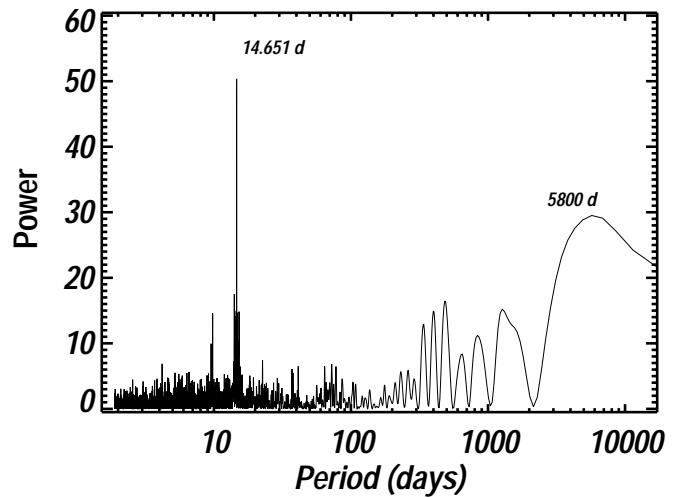

FIG. 5.—Periodogram of the all of the Doppler-shift measurements of 55 Cancri (shown in Fig. 4). The tallest two peaks are both statistically significant at $P = 14.65$ and $P = 5800$ days.

variations are well above the uncertainties, implying that real velocity variations are occurring. During timescales of a few months, the Doppler velocity variations of 55 Cnc are dominated by a 14.65 day periodicity, as reported by Butler et al. (1996). A power spectrum of the entire set of velocities is shown in Figure 5. The strongest peak resides at a period of 14.65 days. This periodicity is the same as that reported by Butler et al. and is caused by a planetary mass companion having $M \sin i = 0.84 \; M_{\mathrm{JUP}}$ in a nearly circular orbit ($e = 0.02$) with semimajor axis of 0.11 AU.

To test the integrity of a single-planet model for 55 Cnc, we fitted all the velocities with a simple Keplerian model, as shown in Figure 6. The fit reveals the expected period of 14.65 days and velocity semiamplitude of 78 m s^{-1}. The fit is poor, with velocity residuals that exhibit an rms of 39 m s^{-1}, well above the errors of 3–10 m s^{-1}. Indeed, the value of the reduced $\sqrt{\chi_\nu^2}$ is 10. Clearly, the single-planet model is inadequate. Moreover, the residuals to the single-planet model show a monotonic rise from 1989 until 1996 and a

FIG. 4.—Doppler-shift measurements for 55 Cancri from 1988 to 2002. Precision improved from ~10 (1988–1994) to ~4 m s^{-1} (1995–2002). The 14 yr timescale of velocity variations is visible to the eye, along with the short-period variations caused by the 14.65 day period planet.
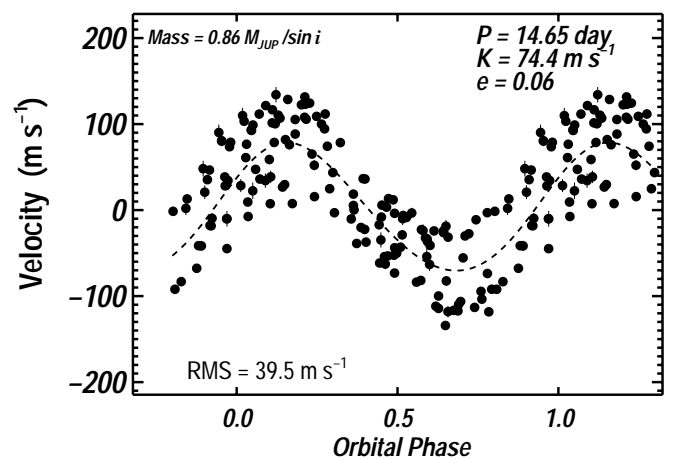

FIG. 6.—Velocities for 55 Cancri, phased at the best-fit period of 14.65 days, which corresponds to the tallest peak in the periodogram (Fig. 5). The dashed line represents the best-fit (single-planet) Keplerian. The rms of 38 m s^{-1} is well above the typical velocity errors of 3–10 m s^{-1}, showing the inadequacy of a single-planet model.

TABLE 2

MEASURED VELOCITIES FOR 55 CANCRI

Jullian Date (−2,450,000)	Radial Velocity (m s⁻¹)	Uncertainty (m s⁻¹)
−2421.2700	26.76	9.7
−2152.9563	4.64	8.4
−1982.3118	32.84	7.5
−1624.3308	−30.37	8.8
−1353.9989	25.15	8.1
−1329.2395	−49.69	10.3
−1093.9639	−14.35	7.2
−1008.0364	−5.64	7.4
−1007.1095	−19.44	7.2
−885.2714	52.52	9.2
−693.9788	84.99	6.4
−650.1551	94.56	9.2
−649.0730	114.22	9.0
−530.3522	138.50	9.0
−323.9368	135.92	5.3
−232.2260	17.73	4.9
−231.1678	1.01	6.0
−206.2017	113.31	3.3
56.9882	127.44	3.8
87.8823	82.81	4.2
88.9186	40.90	3.2
89.0055	40.50	3.5
89.7764	10.12	3.5
89.9859	7.80	3.3
90.7448	−1.91	2.8
90.8930	−4.24	3.6
91.8485	−32.21	3.3
91.9696	−36.71	3.5
120.8739	−18.34	4.2
121.8886	−19.37	3.4
124.8562	17.33	3.5
125.7787	39.75	3.9
126.8369	83.19	5.0
127.8525	103.26	3.8
128.8662	104.70	3.6
144.7105	126.81	3.0
144.8541	112.26	3.2
145.6248	104.37	3.1
145.7650	98.80	3.6
148.8883	16.32	5.2
150.7493	−19.83	3.7
152.6622	−6.85	5.3
168.7494	6.37	7.8
171.7381	96.98	4.6
172.6893	120.98	4.7
173.7246	109.68	3.9
179.7331	−29.13	2.6
180.6884	−27.12	2.8
181.6339	−23.14	3.3
186.7391	116.00	4.9
187.6855	111.31	5.8
199.6818	84.56	4.0
200.7012	107.64	3.9
201.6854	125.87	4.8
202.6895	132.98	3.3
203.6860	128.73	4.8
214.6864	78.00	4.1
215.6724	97.59	4.9
233.6917	116.06	5.7
422.0056	114.70	3.4
437.9283	109.99	2.5
441.9539	0.61	3.4
502.7805	−21.74	3.0
503.7636	−25.69	2.6

TABLE 2—Continued

Jullian Date (−2,450,000)	Radial Velocity (m s⁻¹)	Uncertainty (m s⁻¹)
504.7734	1.33	2.6
536.7737	42.94	4.8
537.7634	80.90	3.5
550.7260	50.93	3.3
563.7190	2.92	4.5
614.6935	78.60	3.3
793.9024	−24.45	3.3
794.9620	−28.09	3.6
831.9320	105.80	3.9
1153.0331	65.36	4.3
1155.0185	80.33	4.1
1206.8777	−51.20	4.2
1212.9279	83.00	4.6
1213.8834	92.76	4.6
1242.7398	86.31	4.2
1298.7216	38.69	4.1
1305.7085	−3.76	4.2
1469.0528	−58.87	7.6
1532.9958	32.55	4.6
1535.0066	63.16	5.4
1536.9490	69.49	3.6
1540.0076	−12.75	4.8
1540.9832	−38.77	5.2
1581.8477	47.97	4.5
1607.8268	40.42	5.1
1626.7339	22.93	4.1
1629.8053	−77.45	4.3
1840.0491	−5.25	6.1
1842.0338	51.73	3.7
1860.0563	29.20	4.2
1861.0366	−5.93	4.2
1872.0209	42.99	7.2
1874.0057	56.46	5.9
1880.0176	−77.99	5.7
1895.0062	−112.16	4.4
1906.9604	−68.84	4.1
1910.8976	−90.13	4.2
1913.9658	−5.69	3.1
1914.9274	13.74	3.1
1927.9088	−13.92	3.3
1945.9059	34.01	2.7
1969.7891	−69.37	4.8
1971.8079	−13.53	4.6
1979.7506	−49.76	4.7
2000.7152	−37.28	5.9
2033.7100	31.16	3.0
2040.6905	−107.42	3.1
2041.6995	−112.83	3.3
2217.0452	−113.73	6.7
2257.0349	−15.85	4.0
2262.9867	−87.66	4.4
2278.9359	−37.02	4.8
2281.9804	38.65	8.3
2285.9884	9.73	4.4
2287.9583	−45.80	5.6
2298.8652	20.02	3.3
2299.7744	1.28	2.4
2306.8041	−113.92	3.4
2315.8035	−18.08	2.9
2316.8553	−48.93	3.3
2333.8160	−95.52	3.2
2334.7307	−105.32	4.2
2335.7892	−99.22	2.3
2338.8319	−5.75	9.1
2345.7838	−57.16	3.8

TABLE 2—*Continued*

Jullian Date (−2,450,000)	Radial Velocity (m s^{-1})	Uncertainty (m s^{-1})
2348.7789	−129.80	3.8
2359.8143	−32.88	4.4
2360.6916	−58.39	5.9
2375.7349	−48.14	4.1
2380.6987	−78.82	4.9
2388.6887	−34.42	2.9
2408.7083	−108.79	3.1
2409.7136	−87.73	5.1
2410.7044	−63.31	4.2
2419.7174	−39.43	4.2
2420.7126	−79.41	3.8
2421.7137	−109.96	3.1
2422.7224	−101.92	3.4
2426.7305	−40.44	2.7
2427.6965	−3.12	3.5
2428.7037	11.76	2.3
2429.7090	11.91	2.3

NOTE.—Table 1 is also available in machine-readable form in the electronic edition of the *Astrophysical Journal.*

subsequent decline (see Fig. 6 in Marcy & Butler 1998). Those residuals exhibit coherent behavior on a timescale of a decade or more. Indeed, the power spectrum in Figure 5 suggests a second period near 5800 days.

4. MODELS OF TWO PLANETS ORBITING 55 CANCRI

We attempted to fit the velocities with a model that consisted of two independent Keplerian orbits representing the inner planet with $P \approx 14.65$ days and a hypothetical outer companion. This double-Keplerian fit is shown in Figures 7 and 8. In Figure 7 the double-Keplerian fit is exhibited after subtracting the long-term velocity variation caused by the outer companion. The velocity residuals have an rms of only
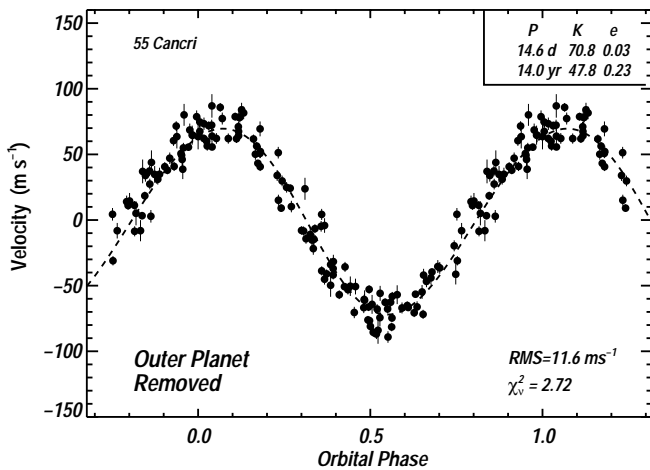

FIG. 7.—Double-Keplerian model (*dashed line*) is fitted to the measured velocities. Here the velocity wobble caused by the outer planet has been removed for clarity, leaving the wobble caused by the inner planet. These residual velocities (*filled circles*) are phased at the 14.65 day period of the inner planet, showing the significant reduction in the residuals compared with Fig. 6. By including a second planet in the model, the rms of the residuals dropped from 39.5 to 11.6 m s^{-1}.
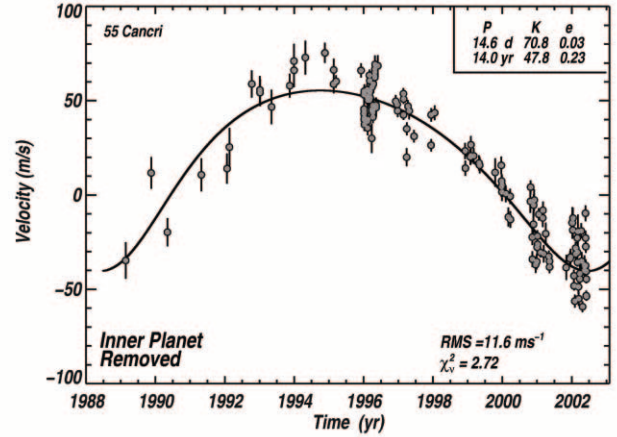

FIG. 8.—Double-Keplerian model (*solid line*) is fitted to the measured velocities (as in Fig. 7). Here the velocity wobble caused by the inner planet ($P = 14.65$ days) has been removed. The residual velocities (*circles*) are plotted vs. time, and the best-fit Keplerian motion of the outer planet has an orbital period of 14 yr. By including a second planet in the model, the rms of the residuals dropped from 38.5 to 11.6 m s^{-1}.

12 m s^{-1} in comparison with the single-Keplerian model (Fig. 6), which had an rms of 39 m s^{-1}. Thus the double-Keplerian model yielded a dramatic improvement in the quality of the fit. Indeed, the value of $\sqrt{\chi_\nu^2}$ fell to 2.7 from the value of 10 achieved with only one planet. This double-planet model is also shown in Figure 8, which exhibits the observed and model velocities after subtracting the effects of the inner planet with its 14.65 days period. Here the wobble of the star caused by the outer planet is revealed more clearly to the eye, although that long-term wobble is apparent in Figure 4 as well.

The double-Keplerian model reveals an outer companion that has period $P = 14 \pm 1.5$ yr, velocity semiamplitude $K = 45 \pm 3$ m s^{-1}, and orbital eccentricity $e = 0.23 \pm 0.06$. The full set of orbital parameters are listed in Table 3. The uncertainties in the orbital parameters are determined by using a Monte Carlo simulation of the velocities, adding artificial velocity noise, and recomputing the double-Keplerian orbital fit. The quality of the double-Keplerian fit suggests that 55 Cnc contains a second companion with an orbital period of 12–16 yr.

From the stellar mass of 0.95 $M_\odot$, the minimum mass of the companion can be computed. We find a minimum mass ($M \sin i$) of 3.5 $M_{\rm JUP}$. The orbital semimajor axis is 5.4 AU.

Clearly, this outer companion was detected previously in the long-term variation in the velocity residuals reported by Marcy & Butler (1998). But only now has enough time passed that the orbit appears to be nearly complete. Figure 8 shows that the velocities, after subtracting the velocity effects of the inner 14.65 days planet, are reaching a minimum, thus indicating the closure of the outer orbit. This orbit closure deserves close examination.

5. THE PERIOD OF THE OUTER PLANET

The period of the outer planet remains somewhat uncertain because the duration of observations, 1989–2002, is only 13 yr, very close to the best-fit period, 14 yr. The most recent season of velocity measurements, during 2002, shows a flattening of the downward slope that had characterized

TABLE 3
TRIPLE-KEPLERIAN ORBITAL PARAMETERS FOR 55 CANCRI

Parameter	Inner "b"	Middle "c"	Outer "d"
Orbital period P (day)	14.653 (0.0006)	44.276 (0.021)	5360 (400)
Velocity amplitude K (m s^{-1})	72.2 (1.0)	13.0 (1.3)	49.3 (2.5)
Eccentricity e	0.020 (0.02)	0.339 (0.21)	0.16 (0.06)
ω (deg)...	99 (35)	61 (25)	201 (22)
Periastron time (JD)..........................	2,450,001.479 (...)	2,450,031.4 (2.5)	2,452,785 (250)
$a_1 \sin i$ (AU)	9.8×10^{-5} (10^{-6})	5.1×10^{-5} (1×10^{-5})	0.0185 (0.002)
$M \sin i$ ($M_{\rm JUP}$)	0.84 (0.07)	0.21 (0.04)	4.05 (0.4)
a (AU)...	0.115 (0.003)	0.241 (0.005)	5.9 (0.9)

the velocity residuals to the single-planet fit for 1996–2001. This flattening of the velocities is visible to the eye in Figure 8.

Nonetheless the flattening is modest, leaving the period of the outer planet weakly constrained. The weak constraint on the period of the outer planet can be illustrated by arbitrarily adopting a period of 20 yr for it instead of the best-fit period, 14 yr. We recomputed the double-Keplerian fit to the velocities but froze the value of the period of the outer planet to be 20 yr. All other orbital parameters for both planets were allowed to float. This constrained fit tests the viability of an orbital period of 20 yr for the outer planet. The resulting $(\chi_\nu^2)^{1/2}$ is 2.92, which is slightly worse than the best-fit value, 2.76. Apparently a 20 yr orbital period is poorer than the best-fit 14 yr period for the outer planet.

However, the value of χ_ν^2 for $P = 20$ yr is only slightly worse than that for the best fit because of dilution caused by the preponderance of measurements during 10 yr prior to the recent season. Adopting $P = 20$ yr yields a poor fit only during the past season. Indeed, during the past two seasons, 2001 and 2002, the velocities appear plausibly fitted by the theoretical curve for $P = 20$ yr, which continues a downward slope. Thus the χ^2 statistic is not a sensitive diagnostic of recent changes in the slope of the velocities.

To improve the sensitivity to the period of the outer planet, we performed a different test of the recent velocities to sense a flattening of the slope. We fitted the velocities with a single Keplerian (with $P \approx 14.65$ days) and a free " trend " in the velocities during two time intervals, 1995.5–2001.5 (yr) and 2000.5–present (2 yr). The trend during those two intervals was found to be -16.25 ± 0.3 m s^{-1} yr^{-1} and -4.5 ± 1.8 m s^{-1} yr^{-1}. Thus, the slope flattened during the past 2 yr from its previous decline rate of 16 to 4.5 m s^{-1} yr^{-1}. The two slopes differ by 6 σ. Isolating just the past season alone (2001.8–2002.5) the best-fit slope is now positive, $+3.4$ m s^{-1} yr^{-1}.

Thus the recent stellar velocities induced by the outer companion are apparently flattening and indeed appear to be increasing. This velocity turnaround is consistent with the best-fit double Keplerian, which yields a period of 14 yr for the outer planet. Nonetheless, the reality of the flattening remains only 6 σ, marginal enough that further intense velocity measurements are warranted. Until then, the period of the outer planet remains poorly constrained and could be as large as 20 yr at the 6 σ level.

5.1. Orbital Eccentricity of the Outer Planet

The orbital eccentricity of the outer planet is formally found to be 0.23 ± 0.06, from the double-Keplerian model.

(In § 6 the superior three-planet model yields an eccentricity of $e = 0.16 \pm 0.06$ for the outer planet.) The uncertainty of 0.06 is the 1 σ standard deviation of 100 Monte Carlo trials in which artificial noise was added to the velocities and the double-Keplerian was recomputed. Clearly, the eccentricity is not constrained well, but is probably less than 0.3.

Our experience is that velocity errors tend to artificially increase the best-fit eccentricity. This artificial increase occurs for at least two reasons. First, the eccentricity cannot be found negative, implying the velocity noise tends to push the best-fit eccentricity away from $e = 0$ in only the positive direction. Second, the flexibility of the shapes of theoretical Keplerian velocity curves allows the best-fit model to be contorted in order to fit the discrepant velocity measurements. Similar issues of the systematic errors and distribution of errors are also discussed by Halbwachs et al. (2000). This Keplerian contortion act is especially insidious for cases in which barely one full orbit has been completed such as this case for the outer planet. The eccentricity is allowed to take on a distorted value to best fit the most recent velocities, bending the velocity curve with a large second derivative. The recent velocity measurements in 2002 are well fitted only by a significant curvature in the orbital fit, as seen in Figure 8. Thus we suspect that the best-fit eccentricity of 0.23 may be overestimated by up to 25%. More careful Monte Carlo tests could be applied to ascertain this bias. Nonetheless, this double-Keplerian fit is clearly not adequate, and the best estimate of orbital parameters likely comes from including a treatment of the periodicity in the residuals.

6. VELOCITY PERIODICITY OF 44 DAYS

The double-Keplerian fit, while a great improvement over a single-Keplerian model, yields residuals with rms = 12 m s^{-1} and $(\chi_\nu^2)^{1/2} = 2.7$. Normal, chromospherically quiet stars yield rms = 4–6 m s^{-1} (partly due to velocity jitter) and yield values of $(\chi_\nu^2)^{1/2}$ less than 1.5. The uncertainties for each velocity measurement are the weighted uncertainty in the mean velocity of the $\sim$400 individual 2 Å spectral chunks from each spectrum. They represent internal errors and closely match the actual uncertainties of the velocities as shown by Cumming et al. (1999). Thus the observed scatter in the residuals to the double-Keplerian fit of 12 m s^{-1} significantly exceeds the errors of $\sim$4 m s^{-1}. The double-Keplerian fit fails to explain the data. We have similarly attempted full N-body simulations of the three-body system (star and two planets). These calculations yield no better fits.
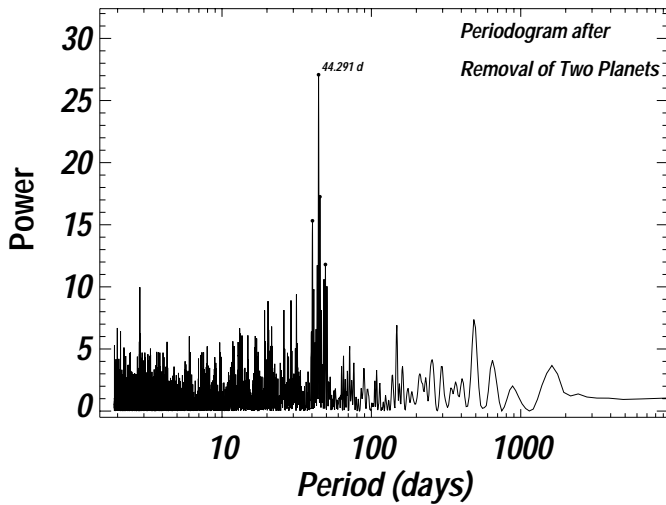
FIG. 9.—Periodogram of the velocity residuals that are left when the predicted velocities of the double-Keplerian model are subtracted from the original velocities. The peak at period 44.3 days has a false alarm probability under 0.1%, implying that the periodicity is real. The cause could be a third planet or permanent inhomogeneities of the velocity field on the stellar surface. The latter is unlikely because 55 Cnc is a quiet star.

A power spectrum of the velocity residuals to the double-Keplerian fit is shown in Figure 9. The power spectrum reveals a strong periodicity at $P = 44.3$ days. This periodicity in the velocities appears compelling even from the velocity measurements obtained within just one season, such as in 1996 and 2002. In principle, this 44.3 days periodicity could be caused by some stellar phenomenon or by a third planetary companion.

We tried triple-Keplerian models to fit the velocities of 55 Cnc, as described in § 6.1. Such models yield $(\chi_\nu^2)^{1/2} = 1.8$, significantly superior to that achieved with only two Keplerian orbits ($(\chi_\nu^2)^{1/2} = 2.7$). We normally find $(\chi_\nu^2)^{1/2} = 1.1$–1.5 for adequate fits to chromospherically quiet stars. Thus the evidence for a third planet is plausible, but it leaves some velocity scatter unaccounted for.

Moreover, the stellar rotation period of 35–42 days is suspiciously similar to this velocity period of 44.3 days. The stellar rotation period, as described in § 2.2, stems directly from observed periodicities in the Ca II chromospheric diagnostic. The period of Ca II emission variations represents the stellar rotation of the latitudes at which the active regions reside. However, during a stellar cycle the active regions probably migrate to other latitudes where differential rotation would yield a different rotation period. Thus, the velocity periodicity at $P = 44.5$ days could, in principle, be caused by surface inhomogeneities (spots, plage, turbulent domains) at a some latitude where the rotation period is $\sim$44 days.

It is difficult to support the notion that surface effects cause the 44 day velocity periodicity in 55 Cnc. The weak chromosphere of 55 Cnc and the lack of photometric variability render its stellar atmosphere stable and void of large velocity excursions, as described in § 2. The velocity jitter is expected to be less than 5 m s^{-1} for such an old, quiet G8 V star. The observed velocity semiamplitude of 13 m s^{-1}, found in the triple-Keplerian fit, is much larger than that expected from surface effects. Thus, a planet explanation is to be favored, with all due concern about the near-coincidence between the rotation and orbital periods of 42 and 44 days, respectively.

6.1. *Interpreting the 44 Day Period as a Third Planet*

The removal of the 14.65 day and 14 yr Keplerian periodicities from the radial velocity data set leaves a large residual scatter with power concentrated at a period of 44.3 days. This velocity signal has a semiamplitude of 13 m s^{-1} (best-fit sinusoid), larger than expected from a chromospherically quiet G8 main-sequence star. Indeed, quiet G8 dwarfs have never revealed any intrinsic periodicity at measurements levels above 5 m s^{-1}, and the velocity jitter (rms) is only 3–5 m s^{-1} for such a star (Saar et al. 1998; Santos et al. 2000) and is observed to be stochastic on yearly timescales. Thus surface effects are expected to cause velocities of lower amplitude and void of coherence, quite different from the amplitude and coherence in the 44.3 day velocity periodicity we observe. The poor plausibility of stellar surface effects in explaining the 44.3 day period motivates a detailed study of triple-planet models here.

The addition of a third planet to the planetary system model results in a stellar reflex motion formed from the sum of three simultaneous Keplerian orbits. The resulting orbital parameters from this best-fit model are listed in Table 3, and the fit is shown in Figure 10. The fit for a triple-Keplerian model gives $(\chi_\nu^2)^{1/2} = 1.8$, an improvement over the two-planet fit, which yielded $(\chi_\nu^2)^{1/2} = 2.7$. This shows that the three-planet model of the planetary system is plausible. This model contains inner and outer planets not very different from the best double-Keplerian model but also contains a middle planet characterized by $P = 44.3$ days, $K = 13.0$ m s^{-1}, and $e = 0.34$, implying $M \sin i = 0.21\ M_{\mathrm{JUP}}$ (see Table 3).

The $(\chi^2)^{1/2} = 1.80$ statistic for the foregoing three-planet model represents a considerable improvement over the two-planet fits to the data. Nevertheless, the 8.5 m s^{-1} velocity scatter of the three-planet fit would require a stellar jitter of $\sim$6.5 m s^{-1}, whereas 55 Cancri likely has a more quiescent jitter of order 3–5 m s^{-1}, as expected for a chromospherically quiet main-sequence star (Saar et al 1998; Santos et al 2000).

One possible explanation for the high χ^2 value in the three-planet model stems from the assumption that the orbits are unperturbed Keplerian ellipses. The system listed in the previous section has a period ratio $P_c/P_b = 3.02$, which is close to $3:1$ commensurability. This means that over the $\sim$5000 day time span that the star has been observed, the planet-planet interactions between the inner and middle planets will tend to add in a constructive way. This is illustrated in Figure 11, which shows the running difference between the radial velocity curve of the star under the influence of summed Kepler motions and under full four-body motion. The discrepancy between the two versions of the stellar motion grows to greater than 100 m s^{-1} after 10 yr of observation, which indicates that self-consistent fitting (as described by Laughlin & Chambers 2001 and Rivera & Lissauer 2002) is required in order to correctly describe a system in this configuration.

We first used a Levenberg-Marquardt minimization routine (Marquardt 1963; Press et al 1992) driving a four-body integrator to produce a self-consistent fit to the radial velocity data. As with other methods based on the method of steepest descent, the Levenberg-Marquardt routine requires a good initial guess in order to converge to a global minimum in the parameter space.

The summed triple-Keplerian fit to the data provides a natural initial guess, just as a dual-Keplerian initial guess
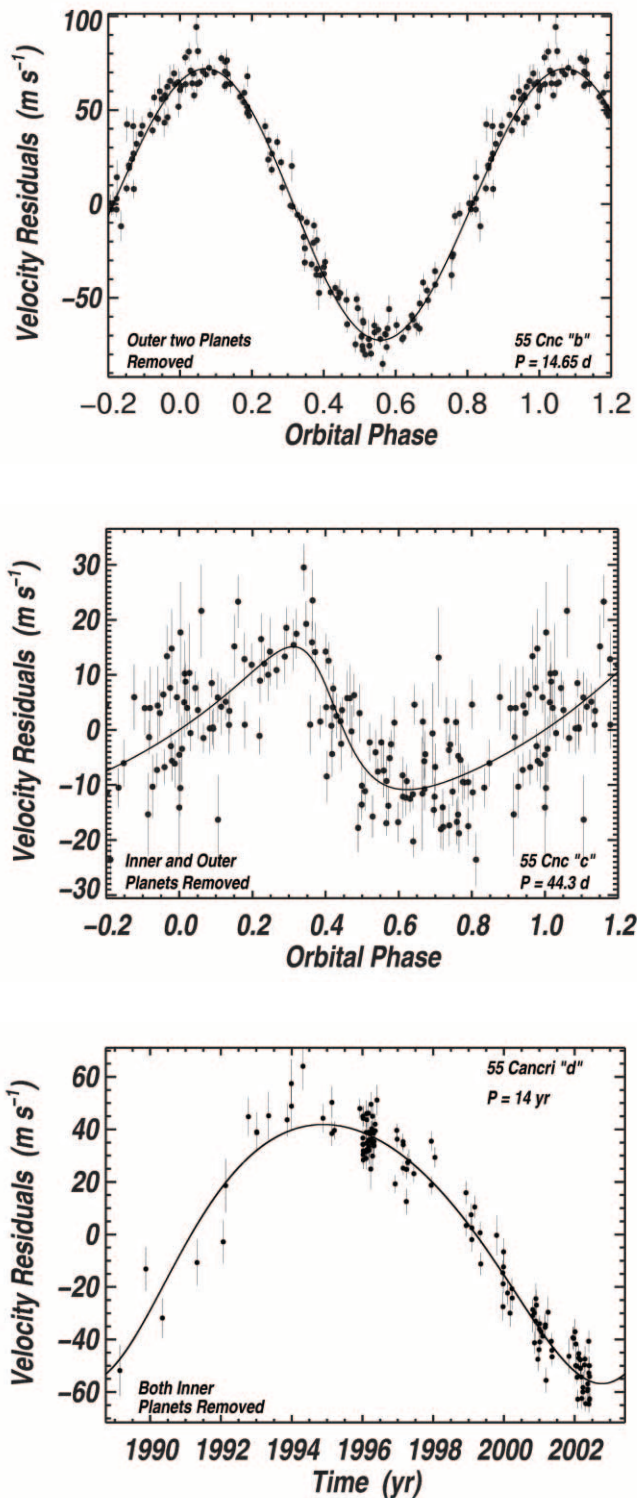
FIG. 10.—Triple-Keplerian orbital fit to the velocities for 55 Cnc. The velocities and fits for each of the three planets are shown separately for clarity by subtracting the effects of the other two planets. The panels contain inner planet b (*top*), middle planet c (*middle*), and outer planet d (*bottom*).

allows the Levenberg-Marquardt method to successfully refine the model of the GJ 876 system (Laughlin & Chambers 2001; Rivera & Lissauer 2001). In that system, the best dual-Keplerian fit (Marcy et al 2001) has $(\chi^2)^{1/2} = 1.88$. When this dual-Kepler fit is used as a starting condition,

the Levenberg-Marquardt method rapidly converges to a fit with $(\chi^2)^{1/2} = 1.55$.

Unfortunately, however, the triple-Keplerian fit to the 55 Cancri data does not provide a similarly propitious point of departure for dramatic improvement. When the summed Keplerian fit is inserted as an initial guess, the code converges to a self-consistent solution with $(\chi^2)^{1/2} = 1.85$. This fit is shown in the first column of Table 4. Experimentation with the starting conditions shows that there is a very strong sensitivity of χ^2 to small variations in the initial conditions, coupled with a χ^2 landscape that is topologically rugged on large scales. It is therefore useful to test additional methods in an attempt to locate the global minimum and thus find the true configuration of the system.

We first used a scheme that turns on the planet-planet perturbations in a gradual way and which was successfully adopted for GJ876 by Rivera & Lissauer (2001). We decreased both the masses of the planets and the magnitudes of the stellar reflex velocities by a factor of 1×10^6. This allows the Levenberg-Marquardt N-body code to recover the triple-Keplerian fit of the previous section. We then gradually increased both the masses of the planets and the radial velocities in a series of discrete increments. After each increment, we allowed the Levenberg-Marquardt minimization to converge to a self-consistent fit. When the radial velocities have grown to their full observed values, the code produces a self-consistent $(\chi^2)^{1/2} = 1.82$ fit, which we list in the second column of Table 4. (All of the fits in Table 4 correspond to epoch JD 2,447,578.730, the time at which the first radial velocity observation of the star was made.)

With the exception of the eccentricity of the middle planet, which has dropped from its large value of 0.34, the osculating orbital elements for the self-consistent fits are quite similar to the summed Kepler fit. In contrast to the situation with GJ 876, the imposition of planet-planet interactions has not improved the χ^2 statistic. Furthermore, examination of the 3:1 resonance arguments, $\theta_1 = 3\lambda_c - \lambda_b - 2\varpi_b$, $\theta_2 = 3\lambda_c - \lambda_b - \varpi_c - \varpi_b$, and, $\theta_3 = 3\lambda_c - \lambda_b - 2\varpi_c$, show that while the model systems are close to resonance, none of the resonance arguments are librating for any of the foregoing fits or for the two additional fits discussed below. This is illustrated in Figure 12, where the time variation of the resonant argument θ_1 is plotted for both the triple-Keplerian fit and for the self-consistent fits. It seems clear that the 55 Cancri system will likely turn out to be very interesting dynamically, even if it is not in resonance today. It likely was in the resonance in the past, and the fact that it is currently not indicates an intriguing past, possibly including tidal dissipation (G. Novak 2002, personal communication).

The failure of the Levenberg-Marquardt routine to significantly improve the χ^2 statistic suggests that a true global minimum in the three-planet parameter space was simply not located by the *locally* convergent Levenberg-Marquardt algorithm. The failure of the Levenberg-Marquardt routine led us to adopt a genetic algorithm (Goldberg 1989) as implemented by D. L. Carroll (1999) for public domain use. The genetic algorithm starts with a population of osculating orbital elements, each referenced to the epoch of the first radial velocity observation. Each set of elements (genomes) describes a unique four-body integration and therefore an associated radial velocity curve for the central star. The fitness of a particular genome is measured by the χ^2 value of its fit to the radial velocity data set. At each generation, the
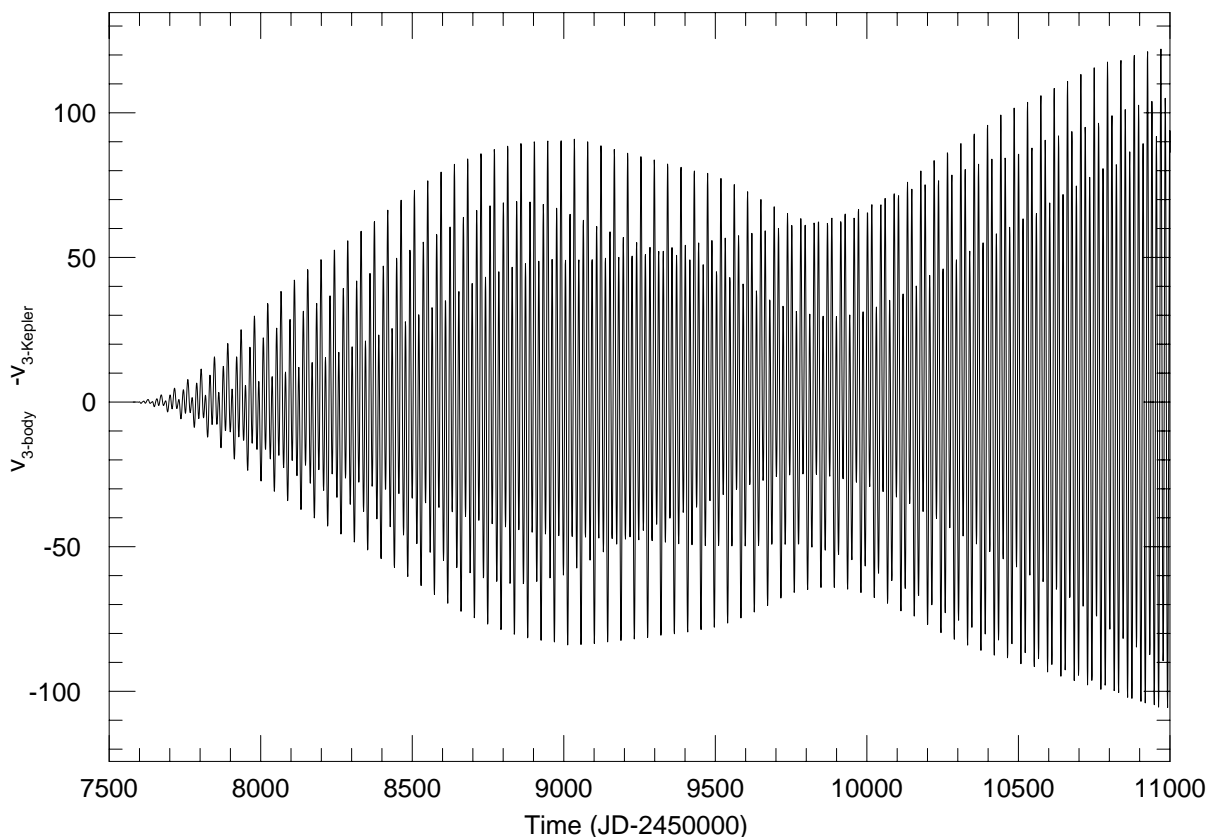
Fig. 11.—Running difference between the radial velocity curve of the star under the influence of summed Keplerian motion, and under the full four-body Newtonian motion. Here three planets are assumed with semimajor axes of 0.11, 0.24, and 5.5 AU, the middle planet remaining hypothetical with period of 44.3 days. The two simulations of stellar motion differ by 100 m s^{-1} after 10 yr, indicating that a self-consistent Newtonian fit will be required if the middle planet with period 44 days actually exists.

genetic algorithm evaluates the χ^2 fit resulting from each parameter set and crossbreeds the best members of the population to produce a new generation.

Extensive use of the genetic algorithm also failed to find a significantly improved χ^2 value over that provided by the summed Keplerian fit, in contrast to the algorithm's excellent performance on test problems involving strongly interacting planets (Laughlin & Chambers 2002). The best fit that we evolved is listed in the third column of Table 4. This fit has $\chi^2 = 1.82$ and has osculating orbital elements

TABLE 4
THREE-PLANET NEWTONIAN MODELS

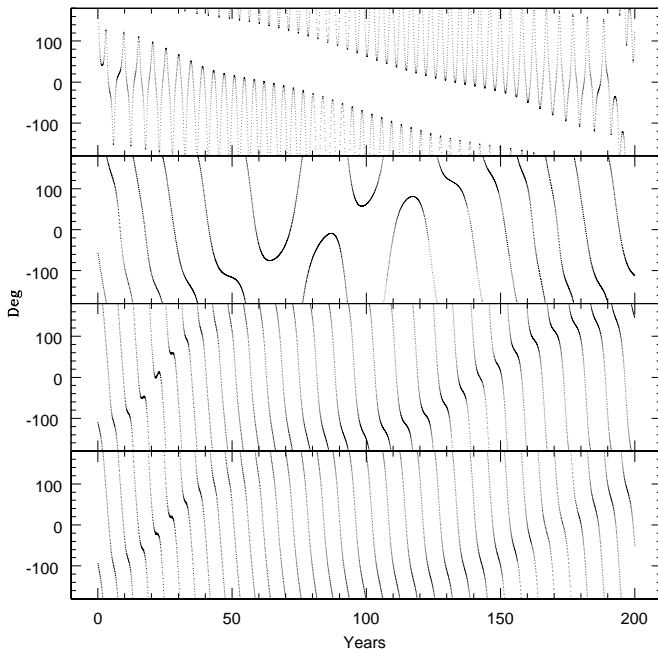|	FOUR-BODY FIT		
PARAMETER	1	2	3
P_b (days)	14.653	14.654	14.653
P_c (days).....................................	44.188	44.241	44.284
P_d (days)	5592.09	5514.33	5483.70
Mean anomaly$_b$ (deg)	247.065	236.105	229.38
Mean anomaly$_c$ (deg)	336.783	215.429	217.71
Mean anomonaly$_d$ (deg).............	5.3461	13.408	9.407
e_b...	0.013	0.039	0.031
e_c...	0.080	0.158	0.142
e_d...	0.146	0.150	0.150
ϖ_b (deg)	93.12	104.17	109.85
ϖ_c (deg).....................................	299.62	51.17	57.77
ϖ_d (deg)	211.67	202.79	205.11
Mass$_b$ ($M_{\rm JUP}$).............................	0.831	0.836	0.837
Mass$_c$ ($M_{\rm JUP}$).............................	0.204	0.202	0.201
Mass$_d$ ($M_{\rm JUP}$).............................	4.363	4.192	4.189
$\sqrt{\chi^2}$..	1.85	1.82	1.82
Epoch (JD)	2,447,578.730	2,447,578.730	2,447,578.730
$v_{\rm epoch}$offset m s^{-1}	3.271	4.038	3.708

Fig. 12.—Time behavior of the 3:1 resonant argument $\theta_1 = 3\lambda_c - \lambda_b - 2\varpi_b$, for a summed Keplerian fit (*first panel*) and self-consistent four-body fits 1 (*second panel*; see Table 4), 2 (*third panel*), and 3 (*fourth panel*). Resonance behavior is not quite achieved in any of these simulations.

that are very similar to the fit obtained by slowly increasing the strength of the planet-planet interactions (second column of Table 4).

The lack of significant improvement in χ^2 with N-body simulations compared with a triple-Keplerian suggests that the interactions are subtle. In none of our N-body simulations did the system of three planets become unstable.

In summary, we have investigated three numerical strategies for producing self-consistent three-planet fits to the 55 Cancri radial velocity data set. All three methods provide fits with χ^2 statistics that are essentially equivalent to the best triple-Kepler fit, and all three fits are in quite good agreement, suggesting that the system lies just outside of the 3:1 resonance. We stress, however, that it is not yet completely clear whether the system is indeed in the 3:1 resonance. Further dynamical fitting and further observation of the star will be required to definitively identify the dynamical relationship between the inner and middle planets.

7. STABILITY OF EARTH-MASS PLANETS NEAR 1 AU

The architecture of the 55 Cancri system, with giant planets in orbits of 14.65, 4680, and (possibly) 44.3 day periods, leads to an anthropocentric question: Is a terrestrial planet stable at 1 AU? The answer is yes. The large period separation between the middle and outer planets admits a broad zone of stable orbits in the so-called habitable zone of this system. We have done a number of representative integrations, which combine the nominal coplanar three-planet system listed in Tables 3 and 4 with an Earth-mass planet on an initially circular 1 AU orbit. The orbital elements are assumed to map onto planetary configuration built in Jacobi coordinates. Apse precession due to general relativis-

tic effects is accommodated by augmenting the stellar gravitational potential with an approximate post-Newtonian correction (see, e.g., Saha & Tremaine 1992). This improvement has a qualitatively negligible effect on the results.

In typical cases, perturbations from the giant planets cause the eccentricity of the Earth-mass planet to oscillate over a 27,000 yr period with an amplitude in e of 0.03. Note that perturbations from the other planets in our own solar system cause Earth to experience chaotic eccentricity oscillations of similar magnitude and duration (see, e.g., Murray & Dermott, 1999).

8. DISCUSSION AND CONCLUSIONS

All ~90 previously reported extrasolar planets reside in smaller orbits than that of Jupiter in our solar system. The duration of Doppler searches for extrasolar planets had not been long enough to capture an entire orbital period of 12 yr for planets at 5 AU. Indeed, all previously known planets are known to have semimajor axes of less than 4 AU, well within Jupiter's orbital distance. Moreover, a large majority of the extrasolar planets reside in eccentric orbits. Thus it has remained inappropriate to compare the extrasolar planets against Jupiter or Saturn in our solar system.

The Lick Observatory Doppler planet search began in 1987 and thus now has the requisite duration to detect planets having orbital periods of over a decade. The velocities of 55 Cnc during 13 yr can be explained nearly adequately by two planets orbiting the star. We had previously detected the inner planet to 55 Cnc ("55 Cnc b"; Butler et al. 1997). Its mass ($>0.9\ M_{\rm JUP}$) and circular orbit with a radius of 0.11 AU from the star represents a class of close-in extrasolar planets, sometimes called "hot Jupiters," the first member of which was 51 Peg (Mayor & Queloz 1995).

The velocities of 55 Cnc now reveal strong evidence of an outer planet at 5.9 AU, previously suspected because of the additional wobble of 55 Cnc (Marcy & Butler 1998). The reality of an outer planet with an orbital period of 13–15 yr and a minimum mass of 4 $M_{\rm JUP}$ is securely supported by the velocities. Remaining velocity residuals with rms of 13 m s^{-1} are caused either by gas motions on the stellar surface or by additional orbiting bodies. The best three-planet fits imply a third planet having $M \sin i = 0.25\ M_{\rm JUP}$ at 0.24 AU in an orbit with $e = 0.3$. But the three-planet models only partially explain the discrepancies in the two-planet fit.

As the first extrasolar planet discovered that orbits farther than 4 AU from its host star, the outer planet to 55 Cnc ("55 Cnc d") is the first one amenable to direct comparison with Jupiter in our solar system. The outer planet has an orbital eccentricity of 0.16 ± 0.06 to be compared with 0.048 and 0.054 for Jupiter and Saturn in our solar system. Thus 55 Cnc d has a modest orbital eccentricity corresponding to an orbital path that carries it as close as 5 AU from the star and as far as 6.8 AU. However, the 55 Cnc system, consisting of three planets as a whole, is clearly qualitatively different from our solar system. The inner two giant planets and their probable migration suggest some difference in formation and history between the two planetary systems.

At a typical angular separation from the star of 0″.47, the planet 55 Cnc d will induce an astrometric wobble in the host star with an amplitude of 1.8 mas $(\sin i)^{-1}$ relative to the barycenter. This gives some hope that *Hipparcos*, the *HST* FGS, or some other ground-based astrometric program could detect the wobble. We carried out an analysis of

the *Hipparcos* and Tycho 2 catalog astrometry similar to that described by Pourbaix (2001) and Pourbaix & Arenou (2001). In some analyses, we used the long term proper motion from Tycho 2 to search for a residual astrometric wobble in the *Hipparcos* astrometry of 55 Cnc. In other analyses we searched for a self-consistent solution of all available astrometry from both *Hipparcos* and Tycho 2. We found no significant wobble in 55 Cnc at a level of ~3 mas over the timescale of the lifetime of *Hipparcos*, 4 yr. However, this time baseline is too short to place any constraints at all on the inclination of the orbit of 55 Cnc d. The wobble of the star caused by it would be nearly linear during 4 yr and hence would be absorbed into the solution of the proper motion of the star. Similarly, no *HST* FGS astrometry has adequate duration. We are unaware of any ground-based astrometry that has adequate precision to detect the companion. Thus we are not able to place any constraints on the orbital inclination of 55 Cnc d and hence cannot place an upper limit on its mass. Both *SIM* and *GAIA* would carry adequate astrometric precision to detect the motion of the star due to 55 Cnc d. But a mission lifetime of at least 7–10 yr (nearly one orbital period) will be necessary to separate the proper motion from orbital parameters. Astrometry having a precision of ~20 μas, coupled with velocities, would constrain the mass of 55 Cnc d to within a few percent.

The velocity residuals to the two-planet model exhibit an rms of 12 m s^{-1} and a strong periodicity of 44.3 days (Fig. 9). These residuals are certainly not due to any instrumental effect, as we are monitoring 300 stars at Lick, including many stars with spectral type G5–K0. No periodicities between 40 and 50 days are seen among those other stars.

The proposition that the 44.3 day period is caused solely by surface effects on the star seems unlikely. The stellar characteristics of 55 Cnc (§ 2) suggest that it is a quiescent star of age 3–8 Gyr, showing very little variation in the usual surface diagnostics. The photometric variation is no more than 1 mmag, and the level and activity in the Ca II K-line emission reversal is small. Such stars are well studied by precision Doppler programs, and they exhibit velocity variations of 2–5 m s^{-1}, presumably caused by turbulence and patchy magnetic regions located nonuniformly over the surface. Thus we cannot support a model in which the velocity residuals with rms of 12 m s^{-1} are intrinsic to the stellar surface.

In contrast, our attempts to fit the velocities, notably the 44.3 day period, with a third planet yielded a significant improvement in the reduced χ^2 compared with that of a simple double-Keplerian fit. Neither a triple-Keplerian model nor a triple-planet Newtonian model succeeded in diminishing the value of χ_ν^2 to a value of 1.0–1.5, instead leaving $\sqrt{\chi_\nu^2} = 1.8$. Moreover, the near coincidence in periods between the 44.3 day velocity period and the 35–42 day rotation period leaves us uncomfortable about the interpretation of the 44.3 day period. Nonetheless, the chromospheric and photometric quiescence of the star is not consistent with stellar surface effects as the cause of the 13 m s^{-1} velocity variations. Indeed, we have never seen such large velocity amplitude and coherence in such a quiet star. This issue is examined carefully by Henry et al. (2002). Thus we favor the model that includes a third planet with that period.

Because the value of χ^2 remains too large, even with a model that contains three planets, one may consider alternative models. Perhaps 55 Cnc contains yet an additional

planet located in the gap between 0.25 and 5 AU. The simulations presented here show that a low-mass planet could persist stably there indefinitely. Planets of sub-Saturn mass located between 0.25 and 5 AU would be difficult to detect securely but would cause velocity variations of a few m s^{-1}, as seen in our velocity measurements.

Another possibility is that rotational modulation of surface inhomogeneities is stronger in metal-rich stars than is seen in solar-metallicity stars. In that case, the 44.3 day period could be caused by stellar rotation after all. Such a hypothesis requires that surface effects both cause a stellar "jitter" of 13 m s^{-1} and remain coherent in phase over timescales of years. This could occur if one longitude maintains its inhomogeneity (spot, magnetic field) for a duration of years.

We also note that the lack of a dust disk (Jayawardhana et al. 2002; Schneider 2001) provides limits to the evolution of debris disks in the face of a giant planet at Jovian distances. One wonders whether such Jupiter analogs tend to enhance the production of dust via enhanced collision rates between the comets and asteroids or instead promote the clearing of the dust due to gravitational perturbations during the lifetime of the star.

The separation of 0".47 between the star and the outer planet makes this system a likely target for future coronographic imaging and interferometric nulling, especially from space-borne telescopes. The outer planet, 55 Cnc d, subtends a fraction of the sky, $f = 1.6 \times 10^{-9}$, as seen from the star. The wavelength-dependent albedo of giant planets in general is under active investigation (Seager & Sasselov 1998; Marley et al. 1999; Goukenleuque et al. 2000; Sudarsky, Burrows, & Pinto 2000). The albedo at visible wavelengths is likely to be ~$\frac{1}{2}$. Thus, one expects the planet, 55 Cnc d, to be fainter than the host star by a factor of 0.8×10^{-9} at optical wavelengths. This implies a contrast of 22.7 mag at V band and an apparent magnitude, $V = 28.7$, for the planet.

With its high abundance of Fe, C, Si, and other heavy elements, along with its age of ~5 Gyr, the 55 Cnc system makes an intriguing environment for questions of organic chemistry and biology. A rocky planet at roughly 1 AU remains a viable prospect dynamically. Moreover, the inner two planets and the outer planet presumably formed from protoplanetary disk material. These extent planets beg the question of the final repository of the disk material that presumably existed between 0.3 and 5 AU. The migration of the inner two planets would not have cleared the region at 1 AU. Indeed, such migration could have occurred by virtue of the two planets delivering angular momentum and energy to the disk material outward of their orbits. Indeed, the presence of two planets at 0.1 and 0.24 AU suggests that material existed between 0.3 and 5 AU, serving as the recipient of their orbital angular momentum.

We expect to detect, within the next 5 yr, a sizable population of Jupiter-mass planets orbiting at 4–6 AU. These planets may serve as signposts of planetary systems characterized by architectures similar to that of our solar system: gas giants beyond 5 AU and rocky planets closer in. Such Jupiters are amenable to direct comparison with Jovian planets in our solar system and will permit characterization of the properties of planetary systems in general.

REFERENCES

Arribas, S., & Martinez Roger, C. 1989, A&A, 215, 305
Baliunas, S. L., Henry, G. W., Donahue, R. A., Fekel, F. C., & Soon, W. H. 1997, ApJ, 474, L119
Baliunas, S. L., et al. 1985, ApJ, 294, 310
Barnes, S. A. 2001, ApJ, 561, 1095
Bell, R., & Branch, D. 1976, MNRAS, 175, 25
Butler, R. P., Marcy, G. W., Williams, E., Hauser, H., & Shirts, P. 1997, ApJ, 474, L115
Butler, R. P., Marcy, G. W., Williams, E., McCarthy, C., Dosanjh, P., & Vogt, S. S. 1996, PASP, 108, 500
Butler, R. P., Vogt, S. S., Marcy, G. W., Fischer, D. A., Henry, G. W., & Apps, K. 2000, ApJ, 545, 504
Cayrel de Strobel, G., Hauck, B., Francois, P., Thevenin, F., Friel, E., Mermilliod, M., & Borde, S. 1992, A&AS, 95, 273
Cayrel de Strobel, G., Soubiran, C., & Ralite, N. 2001, A&A, 373, 159
Cumming, A., Marcy, G. W., & Butler, R. P. 1999, ApJ, 526, 890
Deltorn, J.-M., & Kalas, P. 2002, ApJ, submitted
Dominik, C., Laureijs, R. J., Jourdain de Muizon, M., & Habing, H. J. 1998, A&A, 329, L53
Donahue, R. A., in ASP Conf. Ser. 154, The Tenth Cambridge Workshop on Cool Stars, Stellar Systems, and the Sun, ed. R. A. Donahue & J. A. Bookbinder (San Francisco: ASP), 1235
Donahue, R. A., Saar, S. H., & Baliunas, S. L. 1996, ApJ, 466, 384
Eggen, O. J. 1993, AJ, 106, 1885
Feltzing, S., & Gonzalez, G. 2001, A&A, 367, 253
Ford, E. B., Rasio, F. A., & Sills, A. 1999, ApJ, 514, 411
Fuhrmann, K., Pfeiffer, M. J., & Bernkopf, J. 1998, A&A, 336, 942
Goldberg, D. E. 1989, Genetic Algorithms in Search, Optimization, and Machine Learning (Reading: Addison-Wesley)
Gonzalez, G. 1998, A&A, 334, 221
Gonzalez, G., & Vanture, A. D. 1998, A&A, 339, L29
Goukenleque, C., Bézard, B., Joguet, B., Lellouch, E., & Freedman, R. 2000, Icarus, 143, 308
Greenstein, J. L., & Oinas, V. 1968, ApJ, 153, L91
Habing, H. J., et al. 2001, A&A, 365, 545
Halbwachs, J. L., Arenou, F., Mayor M., Udry, S., & Queloz D. 2000, A&A, 355, 581
Hauck, B., & Mermilliod, M. 1998, A&AS, 129, 431
Henry, G. W. 1999, PASP, 111, 845
Henry, G. W., Baliunas, S. L., Donahue, R. A., Fekel, F. C., & Soon, W. 2000, ApJ, 531, 415
Henry, G. W., Fekel, F. C., Kaye, A. B., & Kaul, A. 2001, AJ, 122, 3383
Henry, G. W., et al. 2002, in ASP. Conf. Ser., Scientific Frontiers in Research on Extrasolar Planets, ed. D. Deming & S. Seager (San Francisco: ASP), in press
Hoffleit, D. 1982, The Bright Star Catalog (New Haven: Yale Univ. Press)
Jayawardhana, R., Holland, W. S., Greaves, J. S., Dent, W. R. F., Marcy, G. W., Hartmann, L. W., & Fazio, G. G. 2000, ApJ, 536, 425
Jayawardhana, R., Holland, W. S., Kalas, P., Greaves, J. S., Dent, W. R. F., Wyatt, M. C., & Marcy, G. W. 2002, ApJ, 570, L93
Laughlin, G., & Chambers, J. E. 2001, ApJ, 551, L109

Laughlin, G., & Chambers, J. E. 2002, Extrasolar Trojans: The Viability and Detectability of Planets in the 1:1 Resonance, N, 124, 592
Lockwood, G. W., Thompson, D. T., Radick, R. R., Osborn,W. H., Baggett, W. E., Duncan, D. K., & Hartmann, L.W. 1984, PASP, 96, 714
Marcy, G. W., & Butler, R. P. 1998, ARA&A, 36, 57
Marcy, G. W., Butler, R. P., Fischer, D., Vogt, S. S., Lissauer, J. J., & Rivera, E. J. 2001, ApJ, 556, 296
Marcy, G. W., Butler, R. P. Williams, E., Bildsten, L. Graham, J. R. Ghez, A. M., & Jernigan, J. G. 1997, ApJ, 481, 926
Marley, M. S., Gelino, C., Stephens, D., Lunine, J. I., & Freedman, R. 1999, ApJ, 513, 879
Marquard, D., 1963, SIAM J. Appl. R., 11, 431
Martell, S., & Laughlin,G. P. 2002, ApJ, submitted
Mayor, M., & Queloz, D. 1995, Nature, 378, 355
Murray, C. D., & Dermott, S. F. 1999, Solar System Dynamics (Cambridge: Cambridge Univ. Press)
Nidever, D. L., Marcy, G. W., Butler, R. P., & Fischer, D. A. 2002, ApJS, 141, 503
Noyes, R. W., Hartmann, L. W., Baliunas, S. L., Duncan, D. K., & Vaughan, A. H. 1984, ApJ, 279, 763
Oinas, V. 1977, A&A, 61, 17
Perrin, M.-N., de Strobel, G. C., Cayrel, R., & Hejlesen, P. M. 1977, A&A, 54, 779
Perryman, M. A. C., et al. 1997, A&A, 323, L49
Pourbaix, D. 2001, A&A, 369, L22
Pourbaix, D., & Arenou, F. 2001, A&A, 372, 935
Press, W. H., Teukolsky, S. A., Vetterling, W. T., & Flannery, B. P. 1992 (2d ed.; Cambridge: Cambridge Univ. Press)
Prieto, C. A., & Lambert, D. L. 1999, A&A, 352, 555
Reid, I. N. 2002, PASP, 114, 306
Rivera, E. J., & Lissauer, J. J. 2001, ApJ, 558, 392
———. 2002, AAS Meeting, 33, 09, 03
Saar, S. H., & Fischer, D. 2000, ApJ, 534, L105
Saar, S. H., Marcy, G. W., & Butler, R. P. 1998, ApJ, 498, L153
Saha, P., & Tremaine, S. 1992, AJ, 104, 1633
Santos, N. C., Israelian, G., & Mayor, M. 2001, A&A, 373, 1019
———. 2000, A&A, 363, 228
Schneider, G. Becklin, E. E., Smith, B. A., Weinberger, A. J., Silversone, M, & Hines, D.C. 2001, AJ, 121, 525
Seager, S., & Sasselov, D. D. 1998, ApJ, 502, L157
Schuster, W. J., & Nissen, P. E. 1989, A&A, 221, 65
Soderblom, D. R. 1982, ApJ, 263, 239
———. 1985, AJ, 90, 2103
Sudarsky, D., Burrows, A., & Pinto, P. 2000, ApJ, 538, 885
Taylor, B. J. 1996, ApJS, 102, 105
———. 1970, ApJS, 22, 177
———. 2002, MNRAS, 329, 839
Trilling, D. E., & Brown, R. H. 1998, BAAS, 30, 1056
Vogt, S. S. 1987, PASP, 99, 1214
Vogt, S. S., et al. 1994, Proc. Soc. Photo-Opt. Instrum. Eng., 2198, 362